A comparison of different methods for modelling the physical human-exoskeleton interface

A comparison of different methods for modelling the physical human-exoskeleton interface

Divyaksh Subhash Chander*

Department of Mechanical and Aerospace Engineering,
Politecnico di Torino,
Corso Duca Degli Abruzzi, 24, 10129 Torino, Italy.
Email: chander.divyaksh@polito.it
*Corresponding Author

Max Böhme[1,2]

1. Faculty of Engineering,
   Leipzig University of Applied Sciences,
   Karl-Liebknecht-Str. 132, 04277 Leipzig, Germany.
2. Faculty V – Mechanical Engineering and Transport Systems,
   Technical University Berlin,
   Straße des 17. Juni 135, 10623 Berlin, Germany.

Email: max.boehme@htwk-leipzig.de

Michael Skipper Andersen and John Rasmussen

Department of Materials and Production,
Aalborg University,
Fibigerstræde 16, 9220 Aalborg Ø., Denmark.
Email: msa@mp.aau.dk
Email: jr@mp.aau.dk

Johannes Zentner

Faculty of Engineering,
Leipzig University of Applied Sciences,
Karl-Liebknecht-Str. 132, 04277 Leipzig, Germany.
Email: johannes.zentner@htwk-leipzig.de

Maria Pia Cavatorta

Department of Mechanical and Aerospace Engineering,
Politecnico di Torino,
Corso Duca Degli Abruzzi, 24, 10129 Torino, Italy.
Email: maria.cavatorta@polito.it

Author

Abstract:

There are several methods to simulate the human-exoskeleton interface but there is insufficient evidence regarding the choice of the method. This work compares two rigid-body methods to simulate the interface: 1) optimization-based contact forces and 2) reaction forces at a point on the interface. Additionally, a method to kinetically align the human-exoskeleton joint axes is presented. A single subject tested an active lower limb exoskeleton in stair ascent. The biomechanical outputs were compared to a baseline model, where the measured assistive and ground reaction force were applied directly to the human model. Both methods showed negligible differences in knee compression force, knee flexion moment, and vastus lateralis activation. However, the ankle outputs showed some differences between the methods. Computationally expensive contact forces provided six-axis interface forces unlike reaction forces, which were limited to the number of constraints required by the exoskeleton. Future studies could compare rigid-body and viscoelastic models.

Keywords:

Human-exoskeleton interface, interaction force, joint misalignment, musculoskeletal model, contact model, contact force

Reference to this paper should be made as follows: Author. (xxxx) 'A comparison of different methods for modelling the physical human-exoskeleton interface', *Int. J. xxxxxxxxxx xxxxxxxxxx*,

Biographical notes: Divyaksh Subhash Chander received his MSc in Automotive Engineering in 2015 and his PhD in Mechanical Engineering in 2021, both at the Politecnico di Torino, Turin, Italy. His PhD thesis focussed on modelling the physical human-exoskeleton interface for the analysis of human-exoskeleton systems using musculoskeletal models. Besides musculoskeletal biomechanics and exoskeletons, his research interests include human factors and ergonomics, and he has participated in research projects concerning both workplace and product ergonomics.

Max Böhme received his MEng degree in Mechanical Engineering at the University of Applied Sciences (HTWK) in Leipzig (2016). He is currently working as a PhD student for both the Technical University Berlin and the HTWK Leipzig. His main research interests are the design of exoskeletons and human biomechanics. The modelling and simulation of both is one of his particular interests. In his current research, he is working on the development of an exoskeleton for elderly people, designed to make it easier for them to climb stairs.

Michael Skipper Andersen received his Master of Science in Electrical Engineering with specialisation in Intelligent Autonomous Systems from Aalborg University in 2004. In 2009, he obtained the PhD degree from the Department of Mechanical Engineering with the thesis title: "Kinematically Over-determinate Musculoskeletal Systems – Modeling, Kinematic analysis and Parameter Identification" within the AnyBody Research Group. Following a short period as Software Engineer in AnyBody Technology, Aalborg, Denmark, he was employed as an Assistant Professor (2009-2012) and later in his current position (2012-) as Associate Professor at Department Materials and Production, Aalborg University, Denmark, with both positions being associated with the Biomechanics research group. The research area of Michael Skipper Andersen

is within musculoskeletal modelling and currently focuses primarily on applying these models within orthopaedics. He has published more than 210 papers in peer-reviewed international journals and national and international conferences.

John Rasmussen is a professor of biomechanics at Aalborg University, Denmark. He is the head and founder of the Biomechanics Research Group at the university's Department of Materials and Production, where he leads research into a number of biomechanical topics in fields such as orthopaedics, sports science, product design, ergonomics and human factors. John Rasmussen is one of the original inventors of the AnyBody Modeling System, and he serves on the board of the spin-out AnyBody Technology. John Rasmussen is a master of science in mechanical engineering and received his PhD from Aalborg University in 1989 in computer-aided design.

Johannes Zentner studied electrical engineering at Tomsk University of Control Systems and Radio-Electronics and then mechanical engineering at Ilmenau University of Technology. He received his doctoral degree in mechanical engineering also in Ilmenau (2005). After that, he worked as assistant professor at Braunschweig University of Technology. Since 2012, he is professor in design engineering at Leipzig University of Applied Sciences. Currently the main objects of research are exoskeletal motion support systems, intralogistics transportation systems with several degrees of freedom, mechanical systems of music instruments. From the scientific point of view, the methodology and technology of design, synergetic design as well as domain spanning modelling and simulation during design process are of interest. One of the current activities is the development of a special exoskeleton for stairs climbing support of elderly people.

Maria Pia Cavatorta is an Associate Professor at the Department of Mechanical and Aerospace Engineering at Politecnico di Torino, Italy. She received her MSc in Mechanical Engineering in 1995 and PhD in Machine Design in 1999 at the same university. From 1997 to 1998, she was a Visiting Scholar at the University at Urbana-Champaign (USA). For the past decade, her research interests have been focused on the integration of human factors and biomechanics into workplace design.

1 Introduction

The increasing interest in exoskeletons is fuelling the development of simulation-based assessment methods. Exoskeletons interact very closely with their users and, thus, the user plays a central role in the design and analysis of exoskeletons. The design and development of exoskeletons is supported through virtual models and musculoskeletal models are a popular choice for that (Agarwal et al. 2016; Tröster et al. 2020). These models allow a detailed investigation of the internal body loads and how an exoskeleton affects those loads.

A key aspect in the simulation of the human-exoskeleton system is the kinetic interaction between the human and the exoskeleton. Generally, the kinetic interaction is simulated through the reaction forces/moments typically associated with the kinematic constraints that connect co-simulation models of the human and exoskeleton models (Ferrati et al. 2013; Agarwal et al. 2016; Guan et al. 2016; Harant et al. 2017; Zhou et al.

2017; Gordon et al. 2018; Jensen et al. 2018; Panero et al. 2020). In a few studies, the interaction forces are solved through force-generating elements that can be configured to simulate point forces (Fournier et al. 2018; Tröster et al. 2018) or rigid-body contact forces (Cho et al. 2012; Jung et al. 2017; Chander and Cavatorta 2019). The force generated by these elements, characterized by a maximum force-generating capacity, is computed through an optimization problem that minimizes a function of the generated force normalized to the maximum capacity of the elements. While the aforementioned references represent the human-exoskeleton interaction through rigid-body models, the actual dynamics at the human-exoskeleton interface requires a more complex model to simulate the soft-tissue on the human side and potentially elastic elements, such as straps or padded braces, on the exoskeleton side. There are examples of viscoelastic models for simulating the human-exoskeleton interface (Schiele 2008; Yandell et al. 2017; Mouzo et al. 2020). A key challenge in using this approach is to obtain accurate estimates of the model parameters, such as the stiffness constant of the human-exoskeleton system, and this is generally overcome by experimental studies with a prototype exoskeleton. Thus, it is difficult to use viscoelastic models in the virtual design phase, but they could be considered for the analysis of prototype or commercial exoskeletons. The analysis of an existing exoskeleton will most likely bring yet another issue into focus, namely misalignment between the human and exoskeleton joint axes. Human-exoskeleton joint misalignment can result in parasitic forces at the interface (Naf et al. 2018; Mallat et al. 2019). One way to account for the effect of the misalignment is to decompose the assistive force of the exoskeleton into an assistive and a dissipative component (Gordon et al. 2018). Furthermore, Gordon et al. 2018 also used the findings of Yandell et al. (2017) to modulate the assistive force profile of the exoskeleton to account for the energy absorption and return dynamics at the interface.

In this work, we focus on rigid-body models as they are generic and can be applied in the virtual design phase to any exoskeleton, unlike viscoelastic models that require interface-dependent parameters. In rigid-body models, the interface force could be simulated as reaction force or as a solution of an optimization problem that minimizes a function of the interface force. There is not sufficient evidence in the literature about the comparison of the two methods. Chander and Cavatorta (2019) compared the two methods of simulating the interface force for a lower limb exoskeleton, the Chairless Chair (noonee GmbH, Germany), and found a difference in the trend of the knee extension moment from the two approaches. The Chairless Chair is a passive sitting support designed for use in an industrial setting and allows for quick, easy and flexible changes between sitting, standing and walking. It consists of two legs and a single load-bearing interface per leg on which the user sits and transfers the bodyweight to the ground. The single interface of the exoskeleton provides a rather static sitting support from only one side of the limb, unlike most exoskeletons that assist in a dynamic activity through multiple interfaces. It is of interest to compare the two rigid-body methods to simulate interface forces in a more generic exoskeleton.

Therefore, the aim of this study was to compare the two rigid-body methods (reaction force associated with kinematic constraints and optimization-based contact force) to simulate the interface of a more generic exoskeleton. Unlike Chander and Cavatorta (2019), the comparison of the two methods in this work is made in the case of an exoskeleton with multiple interfaces in a dynamic activity. The exoskeleton used in this study is an active lower limb exoskeleton that aims to support elderly users in stair negotiation, and consists of interfaces that wrap around the thigh, shank, and foot. The two

methods can, however, lead to different kinematics that can affect their comparison. An additional contribution of this work is to present a method to kinetically align the human and exoskeleton joints to simulate the dynamics while using kinematic data consisting of misaligned joints. Four human-exoskeleton models were developed for the targeted investigation of the two methods of simulating the interface force by negating the difference in kinematics. This work will compare the biomechanical and interface outputs from the four models. The biomechanical outputs were compared to a baseline model that simulated the intended effect of the exoskeleton assistance by applying the assistive torque directly to the human model without using any interface model.

2 Methods

2.1 Exoskeleton

The exoskeleton used in this study is an active exoskeleton consisting of seven parts per leg to form a unilateral rigid system with two rotational joints corresponding to flexion/extension of the knee and dorsiflexion/plantarflexion of the ankle (**Figure 1**). The knee joint of the exoskeleton is actuated while the ankle joint is passive. The segments and joints of the exoskeleton are prefixed with "e-" (e.g.: e-thigh) to avoid confusion with human segments and joints. Three of the seven segments attach to the corresponding human segments and constitute the human-exoskeleton interface: e-thigh, e-shank, and e-foot. These three segments are linked to each other through joints with the remaining four segments in the form of sliding rails. E-thigh, e-shank and e-foot are connected via prismatic joints to thigh rail, shank upper rail and foot rail, respectively. Further, there is a prismatic joint between shank upper rail and shank lower rail. The four rails create the two revolute joints with one degree of freedom (DOF), e-knee (between the thigh rail and shank upper rail) and e-ankle (between the shank lower rail and foot rail). E-knee and e-ankle joints should ideally be coaxial with the human knee and ankle joints respectively. The rails facilitate joint alignment by accommodating users of different anthropometries. The rails allow not only a continuous adjustment of the distance of the e-ankle from the ground and the distance between e-ankle and e-knee but also the relative position of e-shank and e-thigh interfaces from e-knee. Further, e-foot can also be adjusted laterally in the frontal plane.

All three interface components (e-thigh, e-shank, and e-foot) surround the human segments. The anterior side of e-thigh is a rigid structure, whereas two straps, linked through a shaped rigid element, surround the posterior side of the human thigh. The e-shank is made of two rigid parts. One part is a quarter rigid element anterior to the human shank. Medially attached to that part is another rigid shaped element with two straps in between. Two more straps surround the posterior side of the human shank. One of the posterior straps is horizontal and the other one is diagonal from the horizontal band to the e-shank. The e-foot surrounds the foot and consists of a compliant material to allow the foot to roll off. This design is intended to take into account the second DOF in the ankle joint so that lateral movements in the frontal plane are possible to increase the user comfort. All the three interface attachment components are adjustable to consider individual anthropometry and enable the user to fasten the interface himself/herself to increase comfort.

The assistive force to support stair negotiation is implemented through a cable connecting the e-thigh and e-shank, anterior to the human knee joint. An active motor, fixed to the e-thigh, pulls the cable and creates a pulling force. The force vector direction is independent of the knee angle as the cable has a fixed distance from the patella of the knee. The pulling force results in an external moment through the rigid structure of the exoskeleton to support knee extension. This external force is active only if the corresponding leg is in the stance phase of the movement.

2.2 Experiments

The exoskeleton was tested in a laboratory in stair ascent on a custom-built staircase with step height = 160 mm, tread length = 280 mm, and a resulting inclination angle of 30° (**Figure 2**). The staircase consisted of four steps, a stair landing at the upper end and handrails. It also consisted of a force plate (Kistler MiniDyn type 9119AA2, Switzerland) in the second step to record the ground reaction force (GRF). The tensile assistive force in the exoskeleton cable was recorded through a custom-built strain gauge integrated in the e-shank. A marker-based motion capture system (Qualisys AB, Sweden) consisting of twelve active infrared cameras recorded the kinematics at 100 Hz. The software Qualisys Track Manager 2020 was used for recording and synchronization.

The experiments were conducted with one healthy subject (male, 27 years, 77.4 kg, 1.83 m). The subject signed an informed consent prior to participation. Ethical approval for this study was not required. 26 markers were attached to the human body considering characteristic bony landmarks, and 18 markers were attached to each exoskeleton leg (**Figure 3**). Two markers were attached at both shoulders and eight markers were attached medially and laterally at the knee and ankle joints of both the legs for the static trial to determine the joint axes and segment lengths based on the cast model (Cappozzo et al. 1995). No markers could be placed on the human thigh due to the exoskeleton. The distribution of the 18 exoskeleton markers is listed in **Table 1** along with the masses of the exoskeleton segments. Relevant body parameters such as segment lengths, body height and mass were measured first. The exoskeleton was adjusted to the participant's anthropometry as described in **Table 2**.

Before the test was conducted, the participant was able to get familiar with the exoskeleton, donning the exoskeleton on both legs and climbing the stairs several times without recording any data. The subject then carried out 13 ascents, at a self-selected pace, step-over-step and without the use of the handrails. One recording included one ascent, starting with the left leg on the first step (**Figure 2**). After the trials, two static recordings were taken of the subject and exoskeleton in the neutral standing posture. Subsequently, a check for completeness and errors was carried out. Due to the partial occlusion of markers by the testbed, gaps in the trajectories were created. Gaps of up to 10 frames were filled using polynomial interpolation during data preparation. Relational gap filling was used for markers belonging to a cluster. Due to the exclusion of incomplete data series because of incomplete exoskeleton forces or large trajectory gaps, only eight ascents could be analysed.

2.3 Musculoskeletal modelling

The musculoskeletal model was analysed in version 7.3.0 of the AnyBody Modeling System (AMS) (Damsgaard et al. 2006) using the human model available in version 2.3.0 of the AnyBody Managed Model Repository (AMMR) (Lund et al. 2020). The human model used in this work consisted of the leg model based on the Twente Lower Extremity

Model (TLEM) 2.0 (Carbone et al. 2015). The leg model comprised the pelvis, femur, patella, tibia, talus, and foot. The hip joint was defined as a spherical joint, while the knee, patellofemoral, talocrural and subtalar joints were defined as hinge joints with a fixed rotation centre and axis. The pelvis connected to the trunk at the L5S1 joint, which was modelled as a spherical joint. A detailed description of the spine model is provided in de Zee et al. (2007). The arms of the model were disabled as the subject did not use the handrails during the trials.

2.4 Exoskeleton model

The exoskeleton system comprised two separate exoskeletons for the right and left legs, and the methods described in this section were applied to both sides. A computer-aided design (CAD) model of the seven parts constituting the exoskeleton was created. The CAD model was used to estimate the inertia properties of the different parts. Several reference frames were created in the CAD model of the exoskeleton to obtain their precise location and orientation relative to the parts. Reference frames were created for defining and adjusting the rotational and prismatic joints of the exoskeleton inside AMS. Reference frames were also needed for defining the human-exoskeleton interface model, which will be explained subsequently (section 2.6).

The CAD model of the exoskeleton was added to the human model in the multibody environment of AMS by defining the different segments in AMS using the estimated inertia and centre-of-mass along with the measured mass. The prismatic joints of the exoskeleton served to accommodate the user and were adjusted as per the subject's anthropometry (**Table 2**). They were blocked during the trials and constrained in the model to prevent any motion in those joints. Thus, the whole exoskeleton system could be reduced to three segments (e-thigh, e-shank, and e-foot) connected by two revolute joints (e-knee and e-ankle), thereby resulting in eight DOFs for the exoskeleton in the model. The GRF from the trials was applied to the right exoskeleton foot, except in the baseline model where it was applied to the human model. The measured exoskeleton assistance during the trials was synchronized with the movement and read into the model through an external file that stored the magnitude of the force at each time step. The assistive force was applied as tension at the endpoints of the cable and the via points for channelling the cable.

2.5 Baseline model

A baseline model was created, in which there was no interface model between the human and exoskeleton. The GRF and the exoskeleton assistance were directly applied to the human model, bypassing the exoskeleton completely. This baseline model was defined as the ideal assistance (IA) model and simulated the perfect exoskeleton to see its intended effect on the human model. Reference frames were created on the human thigh and shank to reproduce the path of the exoskeleton cable. The assistive force was applied as tension directly at these reference frames on the human segments to simulate the assistance from the exoskeleton. This model ignored the mass and inertia effects of the exoskeleton.

The internal body loads were computed through inverse dynamics analysis of a rigid multibody system together with muscle recruitment to resolve the statically indeterminate system due to the presence of more unknown forces than model DOFs. First, the geometrical parameters of the human model were calibrated to the static trial by using the estimated segment lengths and optimizing the location of the markers on the model (Andersen et al. 2010). Then, the kinematics were solved by reconstructing the movement

of the model from the marker trajectories using a solver for an over-determinate system (Andersen et al. 2009). The inverse dynamics equilibrium equation was set up as:

$$\mathbf{Cf} = \mathbf{d} \tag{1}$$

$\mathbf{C} = [\mathbf{C}^{(M)}\mathbf{C}^{(R)}]$ is the coefficient matrix of the unknown internal forces, $\mathbf{f} = [\mathbf{f}^{(M)T}\mathbf{f}^{(R)T}]^T$, where M and R refer to the muscle and joint reaction forces, respectively. On the right-hand side, $\mathbf{d} = [\mathbf{d}_1^T\ \mathbf{d}_2^T\ \ldots\ \mathbf{d}_n^T]^T$ is the vector of the known external and inertial forces of the different segments. Detailed mathematical description of the equations used in this work and their formulation is available in Damsgaard et al. (2006) and Andersen (2021). The dynamic equilibrium equation (1) would have infinitely many solutions as the number of unknown muscle forces far exceeds the DOFs in the model. Thus, an optimization problem was set up to recruit the muscles (Rasmussen et al. 2001). The optimization problem, also known as the muscle recruitment problem, was framed to minimize a polynomial function of the effort required:

$$\min_{\mathbf{f}} \quad H\left(\mathbf{f}^{(M)}\right) = \sum_{i=1}^{n^{(M)}} \left(\frac{f_i^{(M)}}{N_i^{(M)}}\right)^p \tag{2}$$

subject to:

$$\mathbf{Cf} = \mathbf{d} \tag{3}$$

and

$$f_i^{(M)} \geq 0 \quad \text{for } i = 1 \ldots n^{(M)} \tag{4}$$

Equation (2) is a polynomial function of the normalized muscle forces and power p = 3.0 was used in this work. TLEM 2.0 with cubic polynomial function for muscle recruitment has shown good results in predicting the knee joint contact forces from the fifth grand challenge dataset (Marra et al. 2015). The effort required is measured by the ratio $f_i^{(M)}/N_i^{(M)}$ where $f_i^{(M)}$ is the force produced by the i^{th} muscle and $N_i^{(M)}$ is its strength. This ratio is also known as muscle activity and is used as a measure of the activation of the muscle. In this work, a simple muscle model with constant strength across its functional range was used. Simple muscle model with cubic polynomial muscle recruitment has shown good agreement between estimated muscle activities and measured electromyography data for leg muscles in level and inclined walking (Alexander and Schwameder 2016). Constraint (3) are the equilibrium equations and constraint (4) restricts the muscles to unidirectional force generation, as the muscles can only pull and not push.

2.6 Interface models

2.6.1 Conventional model

In the conventional model, the human-exoskeleton interface forces were simulated using reaction forces typically associated with the kinematic joints between the human and exoskeleton. Constraints were added at each interface between the corresponding human and exoskeleton segments. Reference frames were defined at the centre of the axes of e-thigh and e-shank. The reference frame on the e-foot was defined at the centre of the e-foot base. The reference frames are shown in **Figure 4**. Correspondingly, reference frames were defined on the human segments with the same convention for the axes. At each interface, up to six constraints could be added (three translations and three rotations) between the corresponding human and exoskeleton segments. However, the exoskeleton required eight constraints to fully constrain its eight DOFs. The choice of the eight constraints was a non-trivial problem. As the knee is the target joint of this exoskeleton, maximum constraints

were provided around the knee, that is, on the thigh and shank (**Figure 4**). Three constraints were added at the thigh interface (translation about X and Y; rotation about X). Four constraints were applied at the shank interface (translation about X, Y, and Z; rotation about Y). One constraint was added at the foot interface (translation about Z).

Mathematically, the reaction forces were included as constraints in equation (3) while the normalized muscle forces were minimized by equation (2). Staying true to the approach, the exoskeleton was driven using the kinematic joints instead of the motion capture (mocap) data from the markers on the exoskeleton.

2.6.2 Contact model

The contact model is based on a method developed and verified for GRF prediction (Fluit et al. 2014; Skals et al. 2017). Contact forces were simulated by creating multiple contact detection zones (CDZ) on the exoskeleton and, correspondingly, multiple contact nodes on the human. At each contact node, five unidirectional force-generating contact elements were configured to simulate contact forces, approximating a static Coulomb friction model. One contact element simulated the normal contact force. The remaining four contact elements were arranged in the two shear directions to simulate the positive and negative shear forces. The contact elements in the shear directions were configured such that the generation of the shear force, F_s, was accompanied by the generation of a normal force, F_n, limiting the shear force ($F_s \leq \mu F_n$) by the coefficient of friction, μ. A value of 0.36 was used for the coefficient of friction (Vilhena and Ramalho 2016). Thus, the net normal force was the sum of the forces from the dedicated contact element in the normal direction and the normal components created by the contact elements arranged in the shear directions. Mathematically, with the contact model, the muscle recruitment problem (2) was modified to include the contact elements:

$$\min_{\mathbf{f}} \quad H\left(\mathbf{f}^{(\mathrm{M})}\right) = \sum_{i=1}^{n^{(\mathrm{M})}} \left(\frac{f_i^{(\mathrm{M})}}{N_i{}^{(\mathrm{M})}}\right)^p + \sum_{i=1}^{5n^{(\mathrm{C})}} \left(\frac{f_i^{(\mathrm{C})}}{N_i{}^{(\mathrm{C})}}\right)^p \tag{5}$$

subject to:

$$\begin{aligned} \mathbf{Cf} &= \mathbf{d} \\ f_i^{(\mathrm{M})} &\geq 0 \quad \text{for } i = 1 \ldots n^{(\mathrm{M})} \\ f_i^{(\mathrm{C})} &\geq 0 \quad \text{for } i = 1 \ldots 5n^{(\mathrm{C})} \end{aligned} \tag{6}$$

where **C** is the coefficient matrix of the unknown internal forces **f**; both with additional terms for the unknown contact forces besides the muscle and joint reaction forces. $f_i^{(\mathrm{C})}$ is the force of the i^{th} contact element, $n^{(\mathrm{C})}$ is the number of contact nodes, $N_i{}^{(\mathrm{C})}$ is the strength of the i^{th} contact element. The constraint for the friction force was given implicitly by the linear constraints between four of the five contact elements and these were included in the equation $\mathbf{Cf} = \mathbf{d}$. The GRF prediction method using cubed polynomial muscle recruitment has shown good results in stair descent (Fluit et al. 2014). The strength of the contact elements was set to 6000 N to ensuring low activation cost of the contact elements. The contact elements simulated the contact forces only when the corresponding contact nodes were inside the CDZ. This was implemented by a nonlinear strength function of the contact elements such that the strength was zero when the contact detection threshold was exceeded (Skals et al. 2017). However, it was assumed that the human and exoskeleton remained in contact throughout the motion. This was ensured in the model by increasing the size of the CDZ such that the contact nodes remained within the CDZ throughout the motion.

Reference frames created on the exoskeleton interfaces in the CAD model were used to define the CDZ on the exoskeleton and a corresponding contact node, unique to each CDZ, on the human. For the e-thigh and e-shank interfaces, vertical lines were projected onto the surface of the interface at every 15° from the axis of either interface. Reference frames were created on these projected lines on the interface such that the vertical distance between the reference frames was about 1.8 cm. The foot interface was divided into two distinct regions: the foot base and the foot strap. The CAD model of the foot strap was divided into six surfaces spanning 180° about the foot. These surfaces were used to create a total of 18 reference frames, with each surface consisting of three reference frames spaced approximately 2.4 cm from each other along the midline of the surface. The GRF prediction method was used to simulate the interface forces at the sole or the base of the foot. In total, there were 281 contact points per exoskeleton. Each reference frame had its normal aligned locally to the interface surface at the origin of the reference frame. The second axis of the reference frame was aligned along the length of the interface. The resultant force and moment at an interface were computed by considering the contact force from each contact node of the interface.

In the contact model, the human and exoskeleton models were driven using their respective mocap data. A procedure, like the one used for the kinematics of the human model, was used for the kinematics of the exoskeleton. In the first step, exoskeleton markers were tracked using the over-determinate solver and the position and orientation of the e-shank (6 DOFs) and the angles of the e-knee and e-ankle joints (2 DOFs) were saved for the entire movement. In the second step, these saved values were used as an input to drive the kinematics of the exoskeleton in the inverse dynamics analysis. Using the respective mocap data for the human and exoskeleton resulted in misalignments between the human and exoskeleton joint axes. These misalignments allowed the contact elements to contribute to the flexion/extension of the human joints such that the vastus lateralis and vastus medialis muscles were unrealistically unloaded by the contact elements.

Thus, the misalignments between the human and the exoskeleton joints needed to be removed. This was achieved by adding “dummy segments” in the model to ensure kinetic alignment of the human and exoskeleton joints despite the kinematic misalignment. The dummy segments were used to channel the internal forces of the exoskeleton through a new kinetic path that was aligned with the human leg. They are called dummy segments because they are mass-less, inertia-less segments that do not directly contribute to the dynamics. Three dummy segments corresponding to the human thigh, shank, and foot segments were added in the model to define a dummy leg with dummy knee and ankle joints. The dummy leg was kinematically constrained to the human leg such that the dummy and human joints were perfectly aligned. The inverse dynamics analysis was set up with the following three steps. First, the dummy knee and ankle joints were configured to generate the reaction forces (and moments) in the five constraints of the revolute joint. Second, the reaction forces at the exoskeleton knee and ankle joints were disabled. Finally, reaction forces were added in all six coordinates between the corresponding exoskeleton and dummy segments defining the knee and ankle joints. In this way, a hybrid human-exoskeleton system was created where the exoskeleton joints were kinetically substituted by the dummy joints, which were kinematically aligned with the human joints. The human-exoskeleton interface using the contact model was not modified. The concept is summarized in **Figure 5**. With the human and exoskeleton joints kinetically aligned, the contact elements could not contribute to the flexion/extension of the human joints.

2.6.3 Reference models

The contact and conventional models described above were intended to compare the difference in simulating the interface forces through contact elements and reaction forces. They were respectively denoted as CMDS (Contact Model with Dummy Segments) and KJ (Kinematic Joints). However, the two models also had different kinematics of the exoskeleton. The contact model further required the use of dummy segments to ensure the kinetic alignment of the human and exoskeleton joints. Thus, two reference models were defined to isolate the effects of different kinetics, kinematics, and dummy segments. One reference model introduced dummy segments in the conventional model with the kinematic joints and it was denoted as KJDS (Kinematic Joints with Dummy Segments). In the other reference model, the kinematics of the exoskeleton were driven using the kinematic constraints from the conventional model, while the interface forces were simulated using the contact model with dummy segments and it was denoted as CMKJDS (Contact Model with Kinematic Joints and Dummy Segments). Thus, four interface models (CMDS, KJ, KJDS, and CMKJDS) were defined to compare the two different methods of simulating the interface forces (**Figure 6)** besides the baseline model (**Section 2.5**) that did not model the interface. CMKJDS and KJDS allowed a targeted investigation of the difference between the contact elements and reaction force-based interface model, negating the effects due to the difference in kinematics or the effect of the dummy segments. Instead, CMKJDS and CMDS isolated the effect of the difference in kinematics.

2.7 Analyses

Simulation outputs such as muscle activation, joint moments and joint reaction forces are often used to evaluate the effects of an exoskeleton on the human (Guan et al. 2016; Zhou et al. 2017; Jensen et al. 2018; Tröster et al. 2018; Tröster et al. 2020). The exoskeleton used in this work spanned across the knee and ankle joints, and therefore the outputs concerning these joints were of particular interest. A comprehensive evaluation of the exoskeleton should consider the effect of the exoskeleton on the whole body, but this was beyond the scope of the current work. The activation of vastus lateralis and gastrocnemius, the knee flexion and ankle plantarflexion moments, and the compression force at the knee and ankle were selected as key outputs with a focus on how the interface model affected these outputs. Also of interest were the interface outputs, i.e., the forces in the anterior/posterior, medial/lateral, and proximal/distal directions at each interface from the interface models. Muscle activation data were expressed as a percentage. Joint moment data were normalized to body weight (BW (in N)) and body height (BH (in m)) and expressed as a percentage (Nm/(BW x BH) (%)). Joint reaction force and interface force data were normalized to BW and expressed as a percentage (N/BW (%)).

The stance phase of the right leg was analysed for the eight trials due to the availability of the recorded GRF. Each trial was trimmed, resampled, and normalized to the duration of the stance phase. Each biomechanical output from each model was averaged for the eight trials and plotted on the same graph. The point-based resampling technique (PBRT) was used to create 95% confidence bands about the outputs from the baseline IA model using bootstrapping (Joch et al. 2019). PBRT can be used to check for significant differences in the outputs at each time-step of the movement instead of a single representative value from the curve such as the mean or maximum. Resampling techniques (such as bootstrapping) can assure that the true coverage probability of the confidence bands comes close to the desired nominal level. However, PBRT cannot overcome the limitation of a single subject in the study and statistical significance was therefore not

estimated. Root mean square difference (RMSD) between the interface models (CMDS, KJ, KJDS, and CMKJDS) and IA were calculated for each biomechanical output. Instead, for the interface outputs, the mean and standard deviation of the interface forces from the four interface models were plotted. The baseline model did not have any human-exoskeleton interface force, nor was there any empirical measure to use as a reference for the interface outputs. The kinematic joint models (KJ and KJDS) expressed the resultant forces in the reference frames used for defining the constraints. In the case of contact models (CMDS and CMKJDS), the resultant of the contact forces from all the contact elements of an interface was found at the same reference frame as those from KJ and KJDS.

3 Results

3.1 Biomechanical outputs

Figure 7 shows the time-histories of the selected biomechanical outputs. **Table 3** lists the RMSD between the different interface models and the baseline IA model for these biomechanical outputs.

The activation of vastus lateralis in all the models with the kinematics driven using the kinematic constraints between the human and exoskeleton was lower compared to the ideal case (IA) and the contact model (CMDS) using the marker data for independent human and exoskeleton kinematics. CMDS had the lowest RMSD of 0.67 (+/- 0.07) % in vastus lateralis activation. In fact, CMDS had the lowest RMSD for all the outputs. In the knee flexion moment, the differences between the KJ and CMDS were negligible, and both lay within the confidence bands of the baseline model. Similarly, negligible differences between KJ and CMDS could be observed for the knee compression force. However, KJ showed lower compression force compared to IA around the initial part of the peak. Notably, the curve of KJDS was overlapped by the curve of CMKJDS for all the three outputs about the knee. This was also confirmed by the similar RMSDs shown by KJDS and CMKJDS for the knee outputs.

The outputs concerning the ankle showed a greater inconsistency between the models compared to those about the knee joint. A higher gastrocnemius activation was observed with KJDS compared to the other three interface models. IA lay in between KJDS and the remaining three interface models, such that all the models remained mostly within the confidence interval of IA. Compared to vastus lateralis, CMDS had a higher RMSD of 3.16 (+/- 1.55) % for gastrocnemius activation. CMDS RMSD in gastrocnemius activation was still the lowest amongst four interface models but comparable to the other three models. The conventional model (KJ) showed a reduced effort from the user for ankle plantarflexion moment. For the ankle compression force, KJDS indicated the highest load. Across the three ankle outputs, KJ always required lower effort compared KJDS. Lastly, KJDS and CMKJDS overlapped only for ankle plantarflexion moment and showed notable difference in gastrocnemius activation and ankle compression force.

3.2 Interface outputs

Figure 8 shows the interface forces at the three human-exoskeleton interfaces from the four interface models. The interface forces at the right thigh, shank and foot interfaces are plotted in the local reference frame of each interface (**Figure 4**). The plots represent the force from the exoskeleton to the human.

Firstly, **Figure 8** shows that the kinematic joint models (KJ and KJDS) can only provide limited interface outputs due to the limited number of constraints that could be added in the kinematic joint models. These models assume zero force in the shear directions at the foot and the axial direction at the thigh as no constraints were applied in these directions. Even where the constraints were present, there was a significant difference between the outputs of the kinematic joint models (KJ and KJDS) and the contact models (CMDS and CMKJDS). Secondly, the peak vertical force at the foot interface of the contact models (CMDS and CMKJDS) was substantially closer to the subject weight than that predicted by the kinematic joint models (KJ and KJDS). Thirdly, there was good agreement between CMDS and CMKJDS for all the interface forces except the proximal-distal force at the thigh. Instead, the results between the two kinematic joint models (KJ and KJDS) showed differences in the forces in the anterior-posterior and proximal-distal axes.

4 Discussion

4.1 Biomechanical outputs

Evaluation of assistance quality requires well-defined reference points. Two such points are no assistance and ideal assistance (IA), which span a scale of possibility on which the actual design can be evaluated. The biomechanical outputs of the different interface models were compared with the idealized case, IA, where the exoskeleton assistance was applied directly on the human leg (**Figure 7**). IA was used as a reference case in this work as it had a similar set of assumptions like the interface models used in this study. Specifically, the effects of joint misalignment and compliance at the interface were not considered in this study. These issues, besides other possible issues, would negatively affect the assistance quality received by the user in real life. This means that the biomechanical effort required from the user would be larger in real life than estimated from IA. It is expected that more refined models would deviate from IA but not to a large extent. The difference between IA and the actual use of an exoskeleton should be investigated in future studies focussing more on the interface forces and their measurement, which we did not have the possibility to do.

The biomechanical outputs from the contact model (CMDS) showed good agreement with the IA model in general. CMDS had the lowest RMSD of all the interface models. CMDS also had the same kinematics as IA. KJ, KJDS, and CMKJDS used kinematic constraints between the human and exoskeleton that resulted in different kinematics compared to IA and CMDS. The purpose of using the four interface models was to understand where exactly the difference in results came from.

The biomechanical outputs about the knee, i.e., the activation of vastus lateralis, knee flexion moment, and knee compression force showed consistent results from the different models. Especially, KJDS and CMKJDS showed curves that overlapped each other for the most part as is also evidenced by their similar RMSD for the knee outputs. These models were defined specifically to investigate the differences in the kinetics only and showed that the biomechanical outputs concerning the knee were not affected by the choice between reaction forces or contact elements. However, the presence of dummy segments or the change in kinematics affected the outputs slightly. Notably, the change in kinematics affected the activation of vastus lateralis. CMDS was closest to the ideal assistance, while the other models showed some differences that could be attributed to a change in kinematics (between CMDS and CMKJDS) or a change due to the presence of dummy

segments (between KJ and KJDS). Nonetheless, the general consistency of the different interface models with regards to the biomechanical outputs about the knee joint is a positive result for the overall problem of modelling the physical human-exoskeleton interface. This similarity in the biomechanical outputs about the knee contrasted with the finding of Chander and Cavatorta (2019) for the Chairless Chair, where the two models showed a difference in the knee extension moment trend. The contrasting results could be due to the different nature of the interfaces of the two exoskeletons. An interface that wraps completely around the limb could be better approximated by a kinematic joint than the interface of the Chairless Chair that supports the user from a single side only.

Contrary to the knee outputs, the outputs about the ankle joint showed a greater difference between the reaction force-based models (KJ and KJDS). The notably higher effort required from KJDS compared to KJ highlighted how joint misalignments allowed the muscle recruitment formulation to unload muscles by exploiting reaction forces. KJDS and CMKJDS showed similar results only for the ankle plantarflexion moment. In the activation of gastrocnemius and ankle compression force, CMKJDS was closer to the results of the KJ model rather than the KJDS model. Additionally, CMDS did not match the activation of gastrocnemius by the IA model. Although the difference was not significant, it was greater than the difference between the CMDS and IA models in the activation of vastus lateralis.

We could not identify a reason for the discrepancies in the results concerning the ankle joint. One reason could have been the choice of the kinematic and kinetic constraints. The constraints were chosen to provide ample support about the knee joint and seven of the eight constraints were distributed around the knee: three constraints at the thigh and four at the shank. Two other configurations were tested that had three constraints at the foot and one at the thigh, with the same four constraints at the shank. The biomechanical outputs about the ankle joint changed due to the different kinematics and different support provided by the different constraint configurations. However, they did not necessarily show consistent trends between the four models for the different outputs about the ankle.

4.2 Interface outputs

The contact model simulated contact forces consisting of the normal and shear forces. This was a potential advantage of the contact model over the conventional model that simulated the interface forces as point forces without considering friction. Moreover, the reaction force-based models provided the reaction forces only in the eight added constraints. Thus, only limited information about the interface force was available, which should not be used to make accurate estimates of the interface forces in any case. The interface forces in the limited constraints must compensate for the absence of other constraints. A clear example of this was seen in the vertical forces at the foot and shank. At the foot, the vertical force in the reaction force-based models (KJ and KJDS) was much greater than the body weight of the subject (**Figure 8**). This excessive force was then compensated at the shank. Instead, the contact models (CMDS and CMKJDS) showed much more reasonable forces at the foot interface and correspondingly an excessive vertical force at the shank (relatively speaking) was not observed.

Unfortunately, not much can be said about the validity of the predicted interface forces without experimental measurements of the same. There are examples in literature of experimental measurement of the interface force through six DOF force/torque sensors (Schiele 2008; Zanotto et al. 2015) and computation of the interface force through capacitive pressure sensor matrices (Serrancoli et al. 2019). Experimental measurement of

interface forces highlights how compliance at the interface can affect the user comfort. The interface pressure experienced by the user would depend on the initial strapping pressure, compliance of the soft tissues, and compliance of the interface. The initial strapping (or attachment) pressure has been shown to affect the comfort of the user (Schiele and van der Helm 2009; Langlois et al. 2020). The combined human-exoskeleton compliance at the interface can absorb and release the energy supplied by the exoskeleton during the different phases of the movement (Yandell et al. 2017). Human-exoskeleton misalignments can further affect the interface forces, potentially altering the energy absorbed and released by the compliance at the human-exoskeleton interface.

The contact and conventional models described in this work are rigid-body models that did not model compliance at the human-exoskeleton interface. Compliance at the interface can be accounted for in the model by modifying the assistive force/torque profile of the exoskeleton to compensate for the compliance (Gordon et al. 2018). Alternatively, the compliance can be simulated through the use of calibrated elastic models at the interface (Schiele 2008; Serrancoli et al. 2019). More sophisticated modelling methods, such as force-dependent kinematics (Andersen et al. 2017), could be used in future studies to simulate the elastic compliance at the human-exoskeleton interface in inverse dynamics analysis. Nonetheless, whatever the approach, obtaining accurate estimates of model parameters for simulating human-exoskeleton compliance can be difficult without experiments. This renders the application of these models challenging during the virtual design phase where generic rigid-body models can be used with ease. Once a physical prototype is ready, complex models accounting for compliance at the interface can be used. It is expected that calibrated models simulating compliance will provide more accurate estimates of interface forces than simple rigid-body models. It would be of interest to quantify the difference in the interface force estimates from the two types of models and this could be investigated in a future study with experimental measure of the interface force.

4.3 Dummy segments

In a completely virtual assessment, the exoskeleton joint axes would be perfectly aligned with the human joint axes. However, the use of experimental data from actual trials would almost certainly induce misalignments as opposed to the ideal case of the virtual model. The joint axes' misalignment allowed the contact elements and reaction forces to contribute unintentionally to the movement of the human. This was an unwanted consequence of the computation of the muscle forces through optimization. Small, microscopic misalignments led to disproportionately large mathematical consequences. The solver exploited the contact elements (with practically zero activation cost) and/or reaction forces to unrealistically unload some of the muscles. Thus, dummy segments were introduced between the human and exoskeleton models to kinetically align the exoskeleton joints with the human joints. Alignment between the human and exoskeleton joints could also have been ensured through specific kinematic constraints. However, the dummy segments allowed using the actual mocap data for the kinematics and analysing the aligned kinetics in the same model setup. Once the misalignments were removed kinetically, the exoskeleton worked as an ideal exoskeleton. The contact elements and reaction forces were unable to exploit the misalignments and the model showed reasonable outputs even at high strengths of the contact elements to ensure the low activation of the contact elements. There

was no need to optimize the strength of the contact elements as suggested in Chander and Cavatorta 2020.

However, human-exoskeleton joint misalignment is a real problem that affects the comfort of the user (Naf et al. 2018; Mallat et al. 2019). Joint misalignment has been shown to significantly affect the interface forces (Zanotto et al. 2015). The mocap data from the current study also demonstrated misalignments between the human and exoskeleton. Consequently, a part of the assistive torque from the exoskeleton was dissipated but it was not accounted for in the models with dummy segments. Thus, these models probably overestimated the effect of the assistive torque from the exoskeleton. One way to account for the misalignment in the model is to decompose the assistive torque from the exoskeleton into a functional component and an undesired interaction force (Gordon et al. 2018). The dummy segments can allow splitting the assistive torque into the two components at each time-step of the simulation using the actual misalignment of the current time-step. The effect of the undesired interaction force on the biomechanical outputs could be studied by applying this undesired component additionally to the human model. However, its effect on the interface force cannot be studied through the contact model with the dummy segments. It is of interest to model the effects of joint misalignment, but this was beyond the scope of the current work and future studies could investigate this issue in greater detail.

4.4 Modelling methods

The contact model provided more detailed interface forces than the reaction force-based conventional model. The advantage of the contact model due to the numerous contact elements, however, also came with a greater cost in terms of modelling and computational time compared to the conventional model. The comparison of the two models must be rounded up by a general discussion on using these methods and their key parameters.

The contact model introduces additional parameters in the model such as the number and strength of the contact elements. A higher number of contact nodes (each with five contact elements) can model the interface shape more accurately, and this may improve the results of the simulation, especially when the contact elements are used to model the key features of the interface shape. But once these features have been modelled, the gains from the improved accuracy would be marginal and may be outweighed by the computational cost of every extra contact node. The other parameter of the contact model, i.e., the strength of the contact elements, depends on the exoskeleton. The contact forces are estimated through the muscle recruitment formulation, and they can influence the recruitment of the muscles. Generally, the strength of the contact elements should be high enough to ensure their low activation (Skals et al. 2017). This allows the solver to still minimize the muscle forces while estimating the contact forces, which should be of practically no cost in the objective function. However, the low activation cost of the contact elements could also be exploited to unload the muscles. In this work, the dummy segments ensured that there was no interaction between the contact elements and muscles, and the maximum activation of the contact elements was less than 0.1%. However, in the case of the Chairless Chair, the strength of the contact elements affected the biomechanical outputs and there was a need to optimize strength of the contact elements (Chander and Cavatorta 2020). A maximum activation of 1.5% for the contact elements was reported in the most demanding case of the parametric study (Chander and Cavatorta 2020). The recruitment of the contact elements can also be affected by the muscle recruitment criterion, and this should be tested even though changes in the recruitment criterion have shown negligible differences in GRF

prediction (Fluit et al. 2014). Thus, the contact elements can influence the results from the simulation in several ways and a critical evaluation of the results is necessary.

The conventional model, using kinematic constraints, also introduces an additional parameter in the model, i.e., the choice of constraints amongst the several possible combinations. An exoskeleton introduces additional DOFs in the model that must be constrained by an equal number of constraints. Mathematically, there could be several ways to add the required number of constraints. The chosen constraints must allow the correct transfer of exoskeleton assistance to the user. Changing the distribution of the constraints can alter the biomechanical outputs from the simulation as was mentioned in section 4.1. Thus, a careful consideration of the parameter introduced by the conventional model is also necessary.

In terms of modelling and computational cost, the conventional model holds an advantage. Kinematic constraints and reaction forces require specifying two reference frames and the type of constraint to model the interface. The contact model, on the other hand, requires significantly more effort for developing the model. Multiple reference frames must be defined to capture the shape of the interface. The process of defining multiple reference frames can be faster if parametric surfaces, such as a cylinder, are used to represent the interface. However, that is often not the case with intricately shaped interfaces requiring a manual definition of the reference frames. Next, the contact model must be implemented multiple times at each of these reference frames. This requires specifying the parameters of the contact elements at each reference frame. The process can be accelerated by using programming shortcuts such as a custom class or function. Lastly and optionally, the results of all the contact elements must be aggregated to compute the resultant interface force and moment. Clearly, the contact model requires more steps to prepare the model compared to the conventional model. However, it can be challenging to quantify the difference in model preparation time due to its dependence on the simulation tool and the skill of the user of the tool.

Computational time is also a relevant aspect when considering the difference between the two models. The contact model adds several contact elements in the muscle recruitment optimization problem of the model. This can significantly increase the computational time. In this work, batch processing was used to sequentially run parameter identification on a standing reference trial followed by the kinematics and inverse dynamics analysis of the eight trials. The simulations with the contact model took more than three times the time required than those with the conventional model. Moreover, the contact model also requires a greater memory overhead to load and run the model due to the additional contact elements and reference frames compared to the conventional model. This can be relevant in case parallel processing is used to reduce the computational time. The trade-off between accuracy and computational cost depends on several factors. It depends on the shape of the interface. Simple shapes, like a cylinder, would require fewer contact nodes than intricately contoured shapes. It depends on the purpose of the analysis and the required accuracy of the interface shape for the analysis and, more generally, on the available resources. A preliminary investigation to optimize, for example, the assistive torque from an exoskeleton may benefit more from the time saved with a crude representation of the interface using a few contact elements or reaction forces. Instead, an investigation to optimize the interface shape may benefit more by an accurate representation of the interface shape using several contact elements.

4.5 Limitations

A limitation in this study was the kinematics of the human and exoskeleton feet. The human foot partially penetrated the exoskeleton foot in the model. There could be two reasons for this. Firstly, the recording of the mocap data for the feet was not optimal. Occluded markers were more frequent at the feet than elsewhere on the leg. The presence of the stairs during the trials possibly led to the occlusion of the markers placed at the human and exoskeleton feet. Secondly, the model of the exoskeleton foot was a rather simplified model of the actual exoskeleton foot. The actual exoskeleton foot interface was made of a compliant material to allow some lateral movement of the foot in the frontal plane, and this was not considered in the model. The simplified model might have also led to some errors in the relative location of the markers of the exoskeleton foot in the model and, thus, the reconstruction of the marker trajectories. The consequence of the errors in the kinematics would have reflected in the biomechanical outputs, perhaps more so in the outputs concerning the ankle joint.

Another limitation of this study was data collection with a single subject only. Multiple subjects would have provided a greater insight into the inconsistency reported for the outputs about the ankle joint and, generally, a greater confidence in the findings of this study.

5 Conclusion

Human-exoskeleton interaction plays an important role in the co-simulation of the human-exoskeleton system. There are several methods in the literature to simulate the kinetic interaction between the human and exoskeleton. This study contributes to state-of-the-art by comparing two methods of simulating the human-exoskeleton interface. In one method, the interface force was estimated as rigid-body contact force accounting for static friction through an optimization problem that minimized a cubic function of the normalized force generated by the contact elements. In the other method, the interface force was estimated as reaction force at a single point associated with the kinematic joint constraints at the interface. This study showed consistent biomechanical outputs concerning the knee, the target joint of the exoskeleton, from both the models. However, inconsistencies between the methods were also seen in the outputs concerning the ankle, the reason for which could not be identified.

Further, this work presents a new method to ensure kinetic alignment between the human and exoskeleton joint axes while using kinematic data containing misalignment. This method allows using the same model setup to study the misaligned kinematics and the aligned kinetics. The work highlights practical issues that affect the human-exoskeleton interface force and the limitations of rigid-body methods to tackle them. Misalignment and viscoelastic properties of the actual interface affect the interface force and comfort of the user. These issues would play a key role in a study attempting to validate the interface force predicted by the generic rigid-body models discussed in this study. While rigid-body models are simpler to apply, they sacrifice accuracy compared to viscoelastic models that, on the other hand, would require significantly more efforts to obtain accurate estimates of model parameters. It could be worth investigating the difference between rigid and viscoelastic models in future studies.

Title

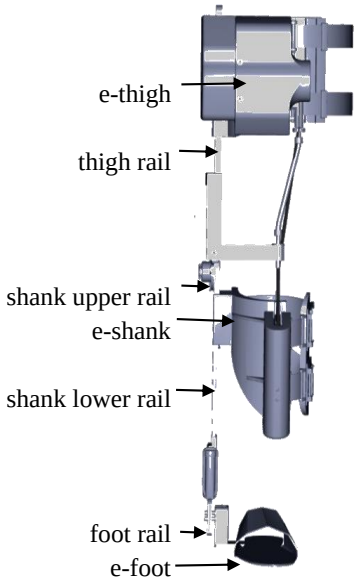

Figure 1: Active exoskeleton to support stair negotiation. The figure shows the exoskeleton for the right leg comprising seven general parts.

Author

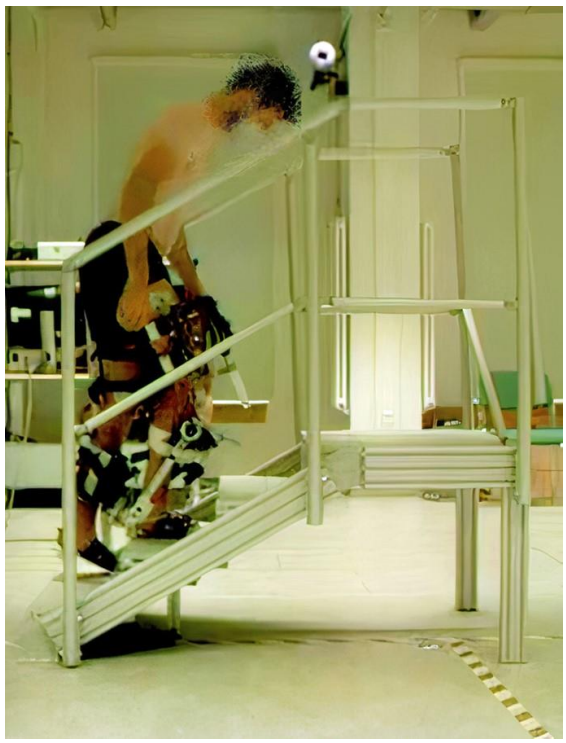

Figure 2: Trial of a stair ascent with the supporting exoskeleton on both legs.

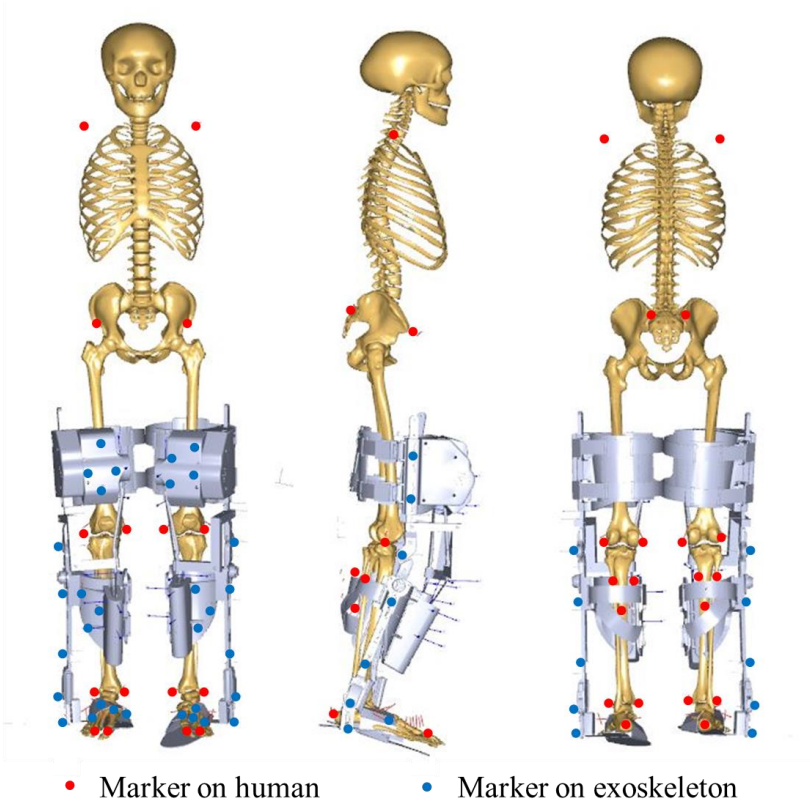

Figure 3: Marker placement on the human and exoskeleton. Markers on human: 2 at shoulders, 4 at pelvis, 4 at knees, 6 at shanks, 4 at ankles, and 6 at feet. Please refer to Table 1 for marker distribution on the exoskeleton

Author

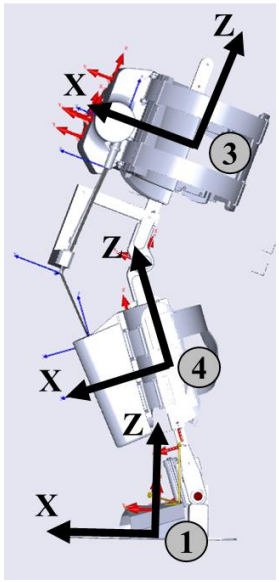

Figure 4: Reference frames on the exoskeleton that were used for defining the kinematic joints. The number in grey circle indicates the number of constraints added at that interface.

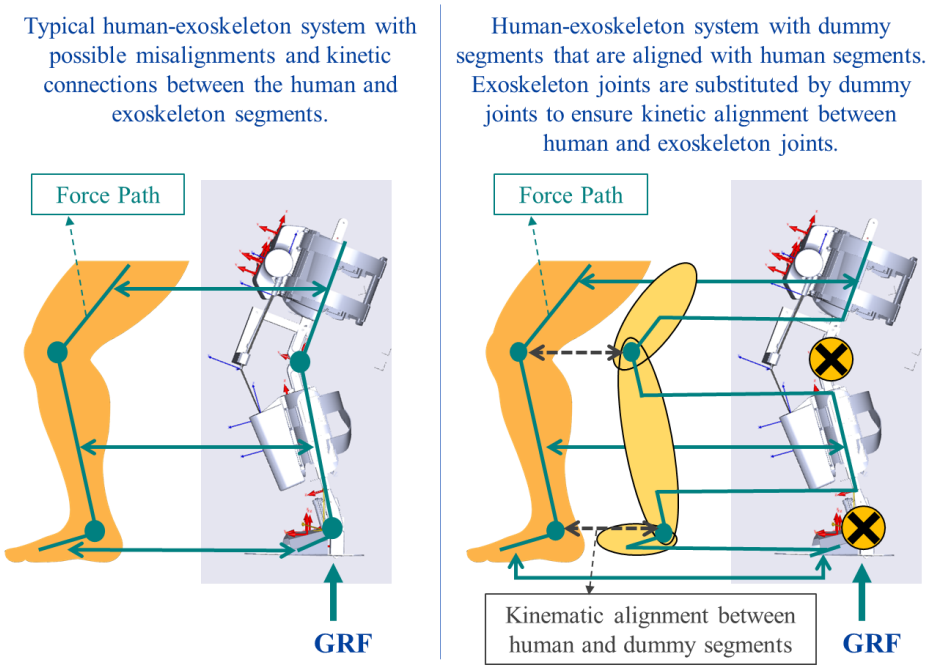

Figure 5: Adding dummy segments in the human-exoskeleton system. On the left is the typical human-exoskeleton system with the kinetic constraints between the human and the exoskeleton. On the right, dummy segments are added to align the exoskeleton joints with the human joints.

Author

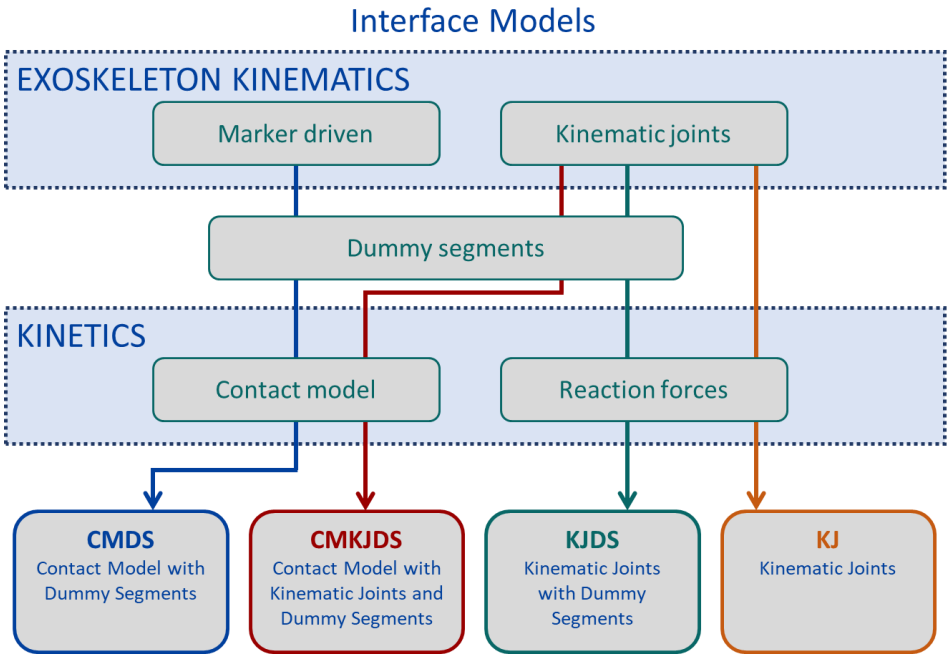

Figure 6: Interface models studied.

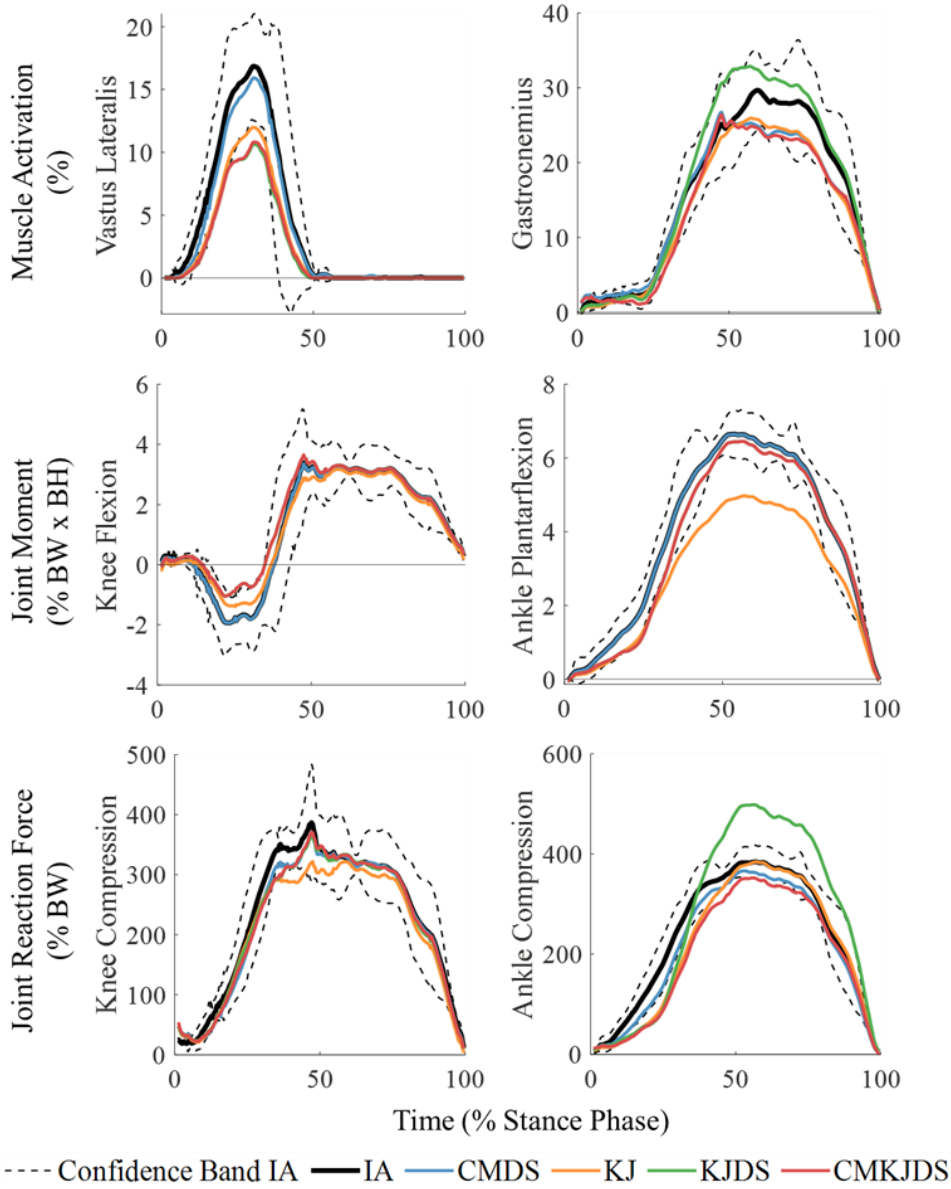

Figure 7: Biomechanical outputs from the Ideal Assistance (IA) reference case and the four interface models (please refer to Figure 6 for the interface models). The confidence bands indicate a 95% confidence interval about the IA.

Author

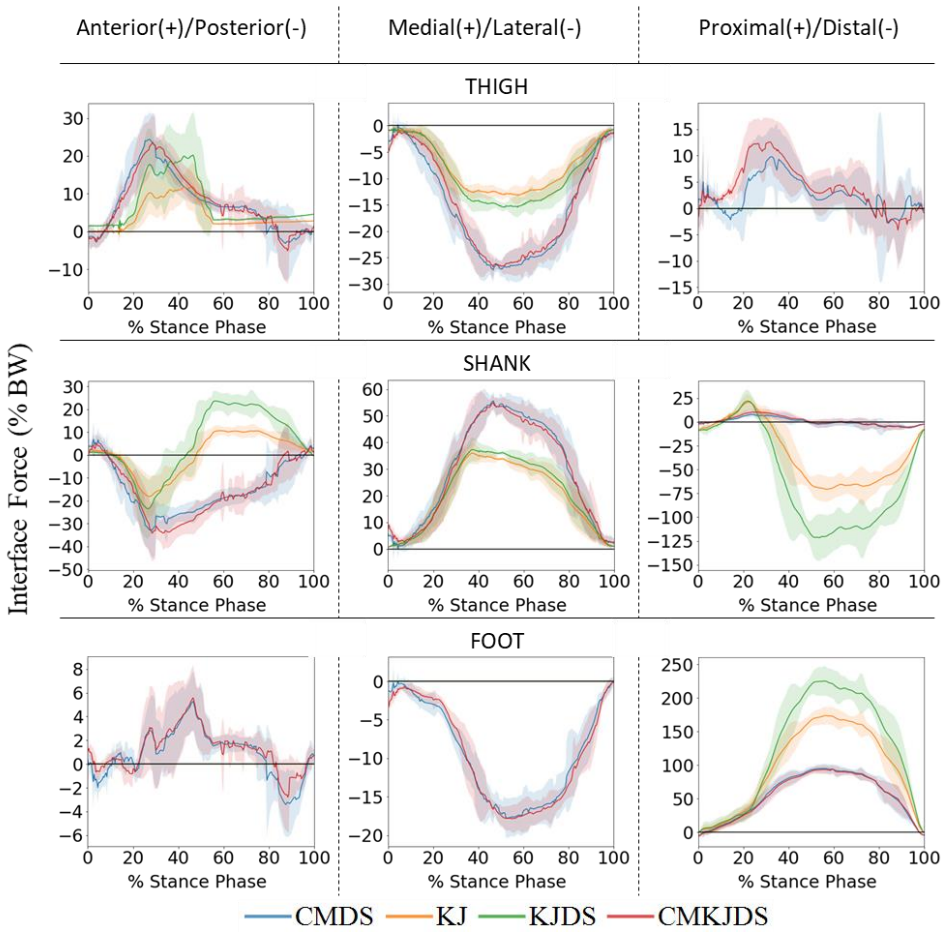

Figure 8: Interface forces from the four different models. Solid lines represent the mean of the eight trials and the shaded region represents +/- 1 std. deviation. Please refer to Figure 4 for the coordinate system and Figure 6 for the interface models.

Title

Table 1: Mass of the exoskeleton parts and marker distribution.

Exoskeleton part	**Mass (kg)**	**Markers per part**
e-thigh	3.56	4
thigh rail	0.82	3 (one at e-knee)
e-shank	1.08	3
shank upper rail	0.17	1
shank lower rail	0.24	2 (one at e-ankle)
foot rail	0.05	1
e-foot	0.17	4

Table 2: Adjusted lengths of the exoskeleton to consider the anthropometry of the subject.

Description of the adjustable length	**Distance (cm)**
Distance between e-foot and foot rail	0.58
Distance between e-ankle and ground	7.5
Distance between e-ankle and e-knee	41.0
Distance between shank upper rail and e-shank	13.5
Distance between thigh rail and e-thigh	2.0

Table 3: RMSD of the biomechanical outputs from the different interface model (CMDS, KJ, KJDS, and CMKJDS) with IA as reference. The results are presented as mean (SD)

Variable	**CMDS**	**KJ**	**KJDS**	**CMKJDS**
Vastus Lateralis Activation (%)	0.67 (0.07)	2.43 (0.26)	3.00 (0.21)	2.91 (0.21)
Knee Flexion Moment (% BW x BH)	0.03 (0.01)	0.36 (0.06)	0.50 (0.04)	0.50 (0.04)
Knee Compression Force (% BW)	17.32 (1.95)	29.95 (2.02)	23.03 (2.01)	23.05 (2.62)
Gastrocnemius Activation (%)	3.16 (1.55)	3.27 (1.38)	3.61 (0.86)	3.66 (1.49)
Ankle Plantarflexion Moment (% BW x BH)	0.01 (0.00)	1.20 (0.11)	0.42 (0.07)	0.42 (0.07)

Author

Ankle Compression Force (% BW)	26.08 (5.67)	40.80 (6.30)	81.14 (9.72)	50.73 (5.80)

References

Agarwal P, Neptune RR, Deshpande AD (2016) A Simulation Framework for Virtual Prototyping of Robotic Exoskeletons. J Biomech Eng 138:061004 . https://doi.org/10.1115/1.4033177

Alexander N, Schwameder H (2016) Comparison of Estimated and Measured Muscle Activity During Inclined Walking. J Appl Biomech 32:150–159 . https://doi.org/10.1123/jab.2015-0021

Andersen MS (2021). Introduction to musculoskeletal modelling. In : Jin Z, Li J, Chen Z. Computational Modelling of Biomechanics and Biotribology in the Musculoskeletal System. Woodhead Publishing. 41-80. https://doi.org/10.1016/B978-0-12-819531-4.00004-3

Andersen MS, Damsgaard M, MacWilliams B, Rasmussen J (2010) A computationally efficient optimisation-based method for parameter identification of kinematically determinate and over-determinate biomechanical systems. Comput Methods Biomech Biomed Engin 13:171–183 . https://doi.org/10.1080/10255840903067080

Andersen MS, Damsgaard M, Rasmussen J (2009) Kinematic analysis of over-determinate biomechanical systems. Comput Methods Biomech Biomed Engin 12:371–384 . https://doi.org/10.1080/10255840802459412

Andersen MS, De Zee M, Damsgaard M, Nolte D, Rasmussen J (2017) Introduction to force-dependent kinematics: Theory and application to mandible modeling. J Biomech Eng 139:091001 . https://doi.org/10.1115/1.4037100

Cappozzo A, Catani F, Della Croce U, Leardini A (1995) Position and orientation in space of bones during movement: anatomical frame definition and determination. Clin Biomech 10:171–178 . https://doi.org/10.1016/0268-0033(95)91394-T

Carbone V, Fluit R, Pellikaan P, van der Krogt MM, Janssen D, Damsgaard M, Vigneron L, Feilkas T, Koopman HFJM, Verdonschot N (2015) TLEM 2.0 – A comprehensive musculoskeletal geometry dataset for subject-specific modeling of lower extremity. J Biomech 48:734–741 . https://doi.org/10.1016/j.jbiomech.2014.12.034

Chander DS, Cavatorta MP (2019) Modelling friction at the mechanical interface between the human and the exoskeleton. Int J Hum Factors Model Simul 7:119 . https://doi.org/10.1504/ijhfms.2019.105434

Chander DS, Cavatorta MP (2020) Modelling interaction forces at a curved physical human-exoskeleton interface. Adv Transdiscipl Eng 11:217–226 . https://doi.org/10.3233/ATDE200028

Cho K, Kim Y, Yi D, Jung M, Lee K (2012) Analysis and Evaluation of a Combined Human-Exoskeleton Model Under Two Different Constraints Condition. Int Summit Hum Simul (ISHS), St Pete Beach, FL, May 23–25

Damsgaard M, Rasmussen J, Christensen ST, Surma E, de Zee M (2006) Analysis of musculoskeletal systems in the AnyBody Modeling System. Simul Model Pract Theory 14:1100–1111 . https://doi.org/10.1016/j.simpat.2006.09.001

de Zee M, Hansen L, Wong C, Rasmussen J, Simonsen EB (2007) A generic detailed rigid-body lumbar spine model. J Biomech 40:1219–1227 . https://doi.org/10.1016/j.jbiomech.2006.05.030

Ferrati F, Bortoletto R, Pagello E (2013) Virtual modelling of a real exoskeleton constrained to a human musculoskeletal model. Lect Notes Comput Sci (including Subser Lect Notes Artif Intell Lect Notes Bioinformatics) 8064 LNAI:96–107 . https://doi.org/10.1007/978-3-642-39802-5-9

Fluit R, Andersen MS, Kolk S, Verdonschot N, Koopman HFJM (2014) Prediction of ground reaction forces and moments during various activities of daily living. J Biomech 47:2321–2329 . https://doi.org/10.1016/j.jbiomech.2014.04.030

Fournier BN, Lemaire ED, Smith AJJ, Doumit M (2018) Modeling and Simulation of a Lower Extremity Powered Exoskeleton. IEEE Trans Neural Syst Rehabil Eng 26:1596–1603 . https://doi.org/10.1109/TNSRE.2018.2854605

Gordon DFN, Henderson G, Vijayakumar S (2018) Effectively Quantifying the Performance of Lower-Limb Exoskeletons Over a Range of Walking Conditions. Front Robot AI 5:1–16 . https://doi.org/10.3389/frobt.2018.00061

Guan X, Ji L, Wang R, Huang W (2016) Optimization of an unpowered energy-stored exoskeleton for patients with spinal cord injury. Proc Annu Int Conf IEEE Eng Med Biol Soc EMBS 2016-Octob:5030–5033 . https://doi.org/10.1109/EMBC.2016.7591857

Harant M, Sreenivasa M, Millard M, Sarabon N, Mombaur K (2017) Parameter optimization for passive spinal exoskeletons based on experimental data and optimal control. IEEE-RAS Int Conf Humanoid Robot 535–540 . https://doi.org/10.1109/HUMANOIDS.2017.8246924

Jensen EF, Raunsbæk J, Lund JN, Rahman T, Rasmussen J, Castro MN (2018) Development and simulation of a passive upper extremity orthosis for amyoplasia. J Rehabil Assist Technol Eng 5:1–10 . https://doi.org/10.1177/2055668318761525

Joch M, Döhring FR, Maurer LK, Müller H (2019) Inference statistical analysis of continuous data based on confidence bands—Traditional and new approaches. Behav Res Methods 51:1244–1257 . https://doi.org/10.3758/s13428-018-1060-5

Jung M, Fau G, Letier P, Mittag U, Zange J, Rittweger J, Runge A (2017) Musculoskeletal Simulation of SOLEUS Ankle Exoskeleton for Countermeasure Exercise in Space. In: González-Vargas J, Ibáñez J, Contreras-Vidal JL, van der Kooij H, Pons JL (eds) Wearable Robotics: Challenges and Trends. Springer International Publishing, Cham, pp 391–396

Langlois K, Rodriguez-Cianca D, Serrien B, De Winter J, Verstraten T, Rodriguez-Guerrero C, Vanderborght B, Lefeber D (2020) Investigating the Effects of Strapping Pressure on Human-Robot Interface Dynamics Using a Soft Robotic Cuff. IEEE Trans Med Robot Bionics 1 . https://doi.org/10.1109/TMRB.2020.3042255

Lund ME, Tørholm S, Jensen BK, Galibarov PE, Dzialo CM, Iversen K, Sarivan M, Marra MA, Simonsen ST (2020) The AnyBody Managed Model Repository (AMMR). https://doi.org/10.5281/ZENODO.3932764

Mallat R, Khalil M, Venture G, Bonnet V, Mohammed S (2019) Human-Exoskeleton Joint Misalignment: A Systematic Review. Int Conf Adv Biomed Eng ICABME 2019-Octob:1–4 . https://doi.org/10.1109/ICABME47164.2019.8940321

Marra MA, Vanheule V, Fluit R, Koopman BHFJM, Rasmussen J, Verdonschot N, Andersen MS (2015) A Subject-Specific Musculoskeletal Modeling Framework to Predict in Vivo Mechanics of Total Knee Arthroplasty. J Biomech Eng 137:020904 . https://doi.org/10.1115/1.4029258

Mouzo F, Michaud F, Lugris U, Cuadrado J (2020) Leg-orthosis contact force estimation from gait analysis. Mech Mach Theory 148: . https://doi.org/10.1016/j.mechmachtheory.2020.103800

Naf MB, Junius K, Rossini M, Rodriguez-Guerrero C, Vanderborght B, Lefeber D (2018) Misalignment Compensation for Full Human-Exoskeleton Kinematic Compatibility: State of the Art and Evaluation. Appl Mech Rev 70:1–19 . https://doi.org/10.1115/1.4042523

Panero E, Muscolo GG, Gastaldi L, Pastorelli S (2020) Multibody Analysis of a 3D Human Model with Trunk Exoskeleton for Industrial Applications. Springer International Publishing

Rasmussen J, Damsgaard M, Voigt M (2001) Muscle recruitment by the min/max criterion - A comparative numerical study. J Biomech 34:409–415 . https://doi.org/10.1016/S0021-9290(00)00191-3

Schiele A (2008) An explicit model to predict and interpret constraint force creation in phri with exoskeletons. Proc - IEEE Int Conf Robot Autom 1324–1330 . https://doi.org/10.1109/ROBOT.2008.4543387

Schiele A, van der Helm FCT (2009) Influence of attachment pressure and kinematic configuration on pHRI with wearable robots. Appl Bionics Biomech 6:157–173 . https://doi.org/10.1080/11762320902879961

Serrancoli G, Falisse A, Dembia C, Vantilt J, Tanghe K, Lefeber D, Jonkers I, de Schutter J, de Groote F (2019) Subject-Exoskeleton Contact Model Calibration Leads to Accurate Interaction Force Predictions. IEEE Trans Neural Syst Rehabil Eng 27:1597–1605 . https://doi.org/10.1109/TNSRE.2019.2924536

Skals S, Jung MK, Damsgaard M, Andersen MS (2017) Prediction of ground reaction forces and moments during sports-related movements. Multibody Syst Dyn 39:175–195 . https://doi.org/10.1007/s11044-016-9537-4

Tröster M, Schneider U, Bauernhansl T, Rasmussen J (2018) Simulation Framework for Active Upper Limb Exoskeleton Design Optimization Based on Musculoskeletal Modeling. Dritte Transdisziplinare Konf 345–353

Tröster M, Wagner D, Müller-Graf F, Maufroy C, Schneider U, Bauernhansl T (2020) Biomechanical model-based development of an active occupational upper-limb exoskeleton to support healthcare workers in the surgery waiting room. Int J Environ Res Public Health 17:1–16 . https://doi.org/10.3390/ijerph17145140

Vilhena L, Ramalho A (2016) Friction of Human Skin against Different Fabrics for Medical Use. Lubricants 4:6 . https://doi.org/10.3390/lubricants4010006

Yandell MB, Quinlivan BT, Popov D, Walsh C, Zelik KE (2017) Physical interface

dynamics alter how robotic exosuits augment human movement: implications for optimizing wearable assistive devices. J Neuroeng Rehabil 14:40 . https://doi.org/10.1186/s12984-017-0247-9

Zanotto D, Akiyama Y, Stegall P, Agrawal SK (2015) Knee Joint Misalignment in Exoskeletons for the Lower Extremities: Effects on User's Gait. IEEE Trans Robot 31:978–987 . https://doi.org/10.1109/TRO.2015.2450414

Zhou L, Bai S, Andersen MS, Rasmussen J (2015) Modeling and design of a spring-loaded, cable-driven, wearable exoskeleton for the upper extremity. Model Identif Control 36:167–177 . https://doi.org/10.4173/mic.2015.3.4

Zhou L, Bai S, Andersen MS, Rasmussen J (2012) Design and Optimization of a Spring-loaded Cable-driven Robotic Exoskeleton. 25th Nord Semin Comput Mech 205–208

Zhou L, Li Y, Bai S (2017) A human-centered design optimization approach for robotic exoskeletons through biomechanical simulation. Rob Auton Syst 91:337–347 . https://doi.org/10.1016/j.robot.2016.12.012